On the decrease of tropical convection with global warming

Nadir Jeevanjee[1]

[1]Geophysical Fluid Dynamics Laboratory, Princeton NJ, 08540

Key Points:

- Three constraints on tropical convection can all be derived analytically from clear-sky subsidence
- Tropospheric mass fluxes at a fixed isotherm should robustly decrease under global warming
- Decreases in anvil cloud area and cloud-base mass flux are not as robust

Corresponding author: Nadir Jeevanjee, nadir.jeevanjee@noaa.gov

Abstract

Tropical convection is expected to decrease with warming, in a variety of ways. Specific incarnations of this idea include the 'stability-iris' hypothesis, as well as the decrease of both tropospheric and cloud-base mass fluxes with warming. This paper seeks to encapsulate these phenomena into three 'rules', and to explore their interrelationships and robustness, using both analytical reasoning as well as cloud-resolving and global climate simulations. We find that each of these rules can be derived analytically from the usual expression for clear-sky subsidence, so they all embody the same essential physics. But, these rules do not all provide the same degree of constraint: the stability-iris effect is not entirely robust due to relatively unconstrained microphysical degrees, and similarly the decrease in cloud-base mass flux is not entirely robust due to unconstrained effects of entrainment and detrainment. Tropospheric mass fluxes, on the other hand, are shown to be well-constrained theoretically, and when evaluated in temperature coordinates they exhibit a monotonic decrease with warming, at all levels and across a hierarchy of models.

Plain Language Summary

Tropical cloudiness is expected to decrease with global warming, in a variety of ways. This phenomenon has a few different manifestations in the literature, whose relationships are unclear. We show analytically that these explanations all embody the same essential physics, but are not equally robust and thus do not all have the same predictive power.

1 Introduction

There is a sense in the literature that tropical convection should 'decrease' with global warming, in various ways. Perhaps the earliest incarnation of this idea is the reduction in the tropical overturning circulation first hypothesized by A. K. Betts and Ridgway (1989), and later demonstrated in global climate models (e.g. Knutson & Manabe, 1995; Vecchi & Soden, 2007). Another, seemingly related manifestation of this idea is that cloud-base convective mass fluxes should decrease with warming, again first noted by Betts (A. Betts, 1998), and later reiterated by Held and Soden (2006) and Vecchi and Soden (2007). More recently, Jenney et al. (2020) found a weakening of convective mass fluxes *throughout* the troposphere, potentially generalizing these earlier results. Finally, Bony et al. (2016) argued via moist thermodynamics and mass conservation that tropical anvil cloud areas should decrease with warming, an argument known as the 'stability-iris' hypothesis. Bony et al. (2016) found evidence for the stability-iris in GCMs, with further evidence found in observations (Saint-Lu et al., 2020) as well as cloud-resolving models (Cronin & Wing, 2017; Beydoun et al., 2021).

A lingering question about all these phenomena, however, is the degree to which they are related. Are they all equivalent somehow, or do their underlying physics differ? For example, the weakening of the tropical circulation and the decrease in tropospheric convective mass flux are governed by changes in the clear-sky subsidence velocity [Eq. (1) below], whereas the decrease in *cloud-base* mass flux is governed by the bulk atmospheric energy budget [Eq. (6) below]. These constraints superficially look different, but at the same time both depend on the difference in how atmospheric radiative cooling and atmospheric moisture scale with global warming. This suggests a potential equivalence between the mechanisms, which has not been pursued or made precise.

Beyond equivalence, there is also the question of whether these phenomena are equally robust. While decreases in circulation strength and convective mass flux with warming seem to occur with few exceptions, the same is not true of the stability-iris effect: some earlier studies with cloud-resolving models found an *increase* of anvil cloud area with warming (Tsushima et al., 2014; Singh & O'Gorman, 2015), with the more recent RCEMIP

intercomparison finding a similar increase in roughly 1/3 of participating models (Wing et al., 2020; Stauffer & Wing, 2022). This diversity amongst models leads to a correspondingly large uncertainty in the associated 'tropical anvil cloud area feedback', whose magnitude and uncertainty range rival those of all other cloud feedbacks (Sherwood et al., 2020).

Given this state of affairs, it seems worthwhile to more closely scrutinize these different manifestations of decreasing convection, assessing both their inter-relatedness and robustness. We attempt this here by encapsulating these phenomena into three 'rules', showing mathematically that they are indeed closely related, and in some cases equivalent. In fact, all three phenomena spring from a common origin, namely the well-known expression (1) for subsidence vertical velocity. The specific mathematical forms of these rules suggest varying degrees of robustness, however, which we evaluate with both global and cloud-resolving simulations.

We focus here on the stability-iris effect (Section 2) and the decrease of convective mass fluxes both throughout the troposphere and at cloud base (Sections 3 and 4), leaving the thornier question of the weakening of large-scale tropical circulations for discussion only (Section 5). The simulations utilized here are primarily cloud-resolving simulations performed with GFDL's FV^3 dynamical core, run in doubly-periodic radiative-convective equilibrium (RCE) over a range of surface temperatures and with non-interactive radiation and a simplified, warm-rain only microphysics scheme. These idealized simulations are supplemented by more comprehensive cloud-resolving simulations with DAM (Romps, 2008), which include full complexity microphysics as well as interactive radiation, as well as 1%CO_2 GCM simulations using GFDL's CM4 (Held et al., 2019). Further details of both sets of cloud-resolving simulations are given in the Appendices.

Subsidence vertical velocity

The expression for the subsidence vertical velocity is derived (e.g. Jenney et al., 2020) by considering the thermodynamic energy equation in clear-skies, i.e. where there is no condensation heating. The only diabatic heat sources are then radiative and evaporative cooling, denoted $\mathcal{H}_{\rm rad}$ and $\mathcal{H}_{\rm e}$ respectively, both negative and in units of K/s. Neglecting horizontal heat transport, the thermodynamic energy equation implies that the steady state clear-sky subsidence velocity $w_{\rm sub} < 0$ is given by

$$w_{\rm sub} \;=\; \frac{\mathcal{H}_{\rm rad} + \mathcal{H}_{\rm e}}{\Gamma_d - \Gamma} \;. \tag{1}$$

Here Γ_d and Γ have their usual meanings as the dry and actual lapse rates, respectively. The difference $\Gamma_d - \Gamma$ is of course due to the presence of moisture, in a sense we will make precise below, so the expression (1) indeed combines information about radiation and moisture. Equation (1) will be the starting point for each of our rules going forward. Note that evaporative cooling $\mathcal{H}_{\rm e}$ is often neglected in calculations of $w_{\rm sub}$, despite the fact that precipitation efficiencies can be 0.5 or less and hence $\mathcal{H}_{\rm e}$ is often equal to or greater than $\mathcal{H}_{\rm rad}$ (Jeevanjee & Zhou, 2022; Lutsko et al., 2022).

2 Stability-iris

We begin with the stability-iris hypothesis of Bony et al. (2016). The subsidence vertical velocity in Eq. (1) is not uniform in the vertical, and thus has a nonzero divergence which must be balanced by a horizontal clear-sky convergence CSC $= \partial_z w_{\rm sub}$, or

$$\text{CSC} \;=\; \partial_z \left(\frac{\mathcal{H}_{\rm rad} + \mathcal{H}_{\rm e}}{\Gamma_d - \Gamma} \right) \;. \tag{2}$$

This horizontal convergence into clear-skies must be balanced by net convective detrainment (or divergence) from cloudy skies, so the above is also an expression for net con-

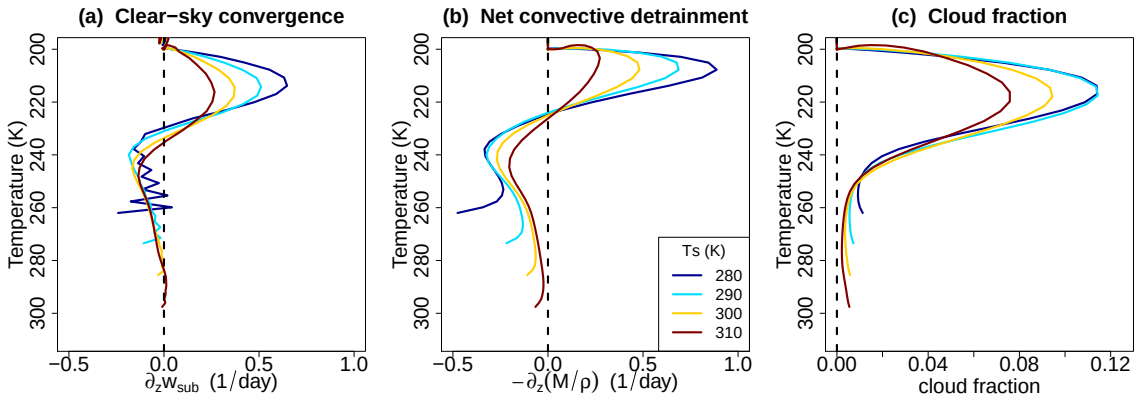

Figure 1. *Simulations results are consistent with the stability-iris hypothesis, but the relationship between CSC/detrainment and cloud fraction is not proportional.* Shown here are simulated profiles of **(a)** clear-sky convergence as diagnosed via Eq. (2) **(b)** convective detrainment $-\partial_z(M/\rho)$ where the convective mass flux M is diagnosed as described in Appendix A, and **(c)** cloud fraction. Panels a and b are similar, as required by mass continuity, and all three panels show a decrease in their upper-tropospheric maxima with warming. But the CSC and detrainment profiles are not sign-definite, whereas cloud fraction is. Here and elsewhere profiles are cut off at cloud base for clarity.

vective detrainment. The stability-iris hypothesis argues that because moist adiabatic lapse rates decrease at a fixed isotherm with surface warming (Fig. A1a), then the denominator in Eq. (2) should increase with warming and hence CSC should decrease. The stability-iris hypothesis further assumes that cloud fraction is in some sense proportional to net convective detrainment, a key assumption which we dwell on below. Combining these arguments for the moment, we then have our first rule for how convection decreases under global warming:

> **Rule 1 (Stability-iris)**: *Clear-sky convergence, net convective detrainment, and anvil cloudiness should decrease together with warming.*

Figure 1 tests this rule by showing profiles of cloud fraction, CSC [diagnosed via Eq. (1)], and net convective detrainment $-\partial_z(M/\rho)$, where M (kg/m^2/s) is the convective mass flux diagnosed via conditional sampling of convecting grid cells (see Appendix for details). These profiles are all drawn from our FV^3 RCE simulations, using temperature as a vertical coordinate since CSC and anvil cloud peaks are well known to follow isotherms much more closely than isobars under global warming (i.e. the 'Fixed Anvil Temperature' hypothesis, Hartmann & Larson, 2002; Hartmann et al., 2019). Figure 1a,b confirms that the profiles of clear-sky convergence and net convective detrainment are roughly the same (as they should be by mass continuity), despite being independently diagnosed. Furthermore, these profiles both show a decrease in their upper-level maxima with warming, as do the cloud fraction profiles in panel c. These results are all consistent with Rule 1 above.

But, Figure 1 does not show a straightforward proportionality between CSC/detrainment and cloud fraction; to the contrary, the CSC/detrainment profiles actually *change sign* in the vertical, as net entrainment in the lower troposphere gives way to net detrainment in the upper troposphere. The cloud fraction profiles are meanwhile positive definite, so the relationship between CSC/detrainment and cloud fraction cannot be a direct pro-

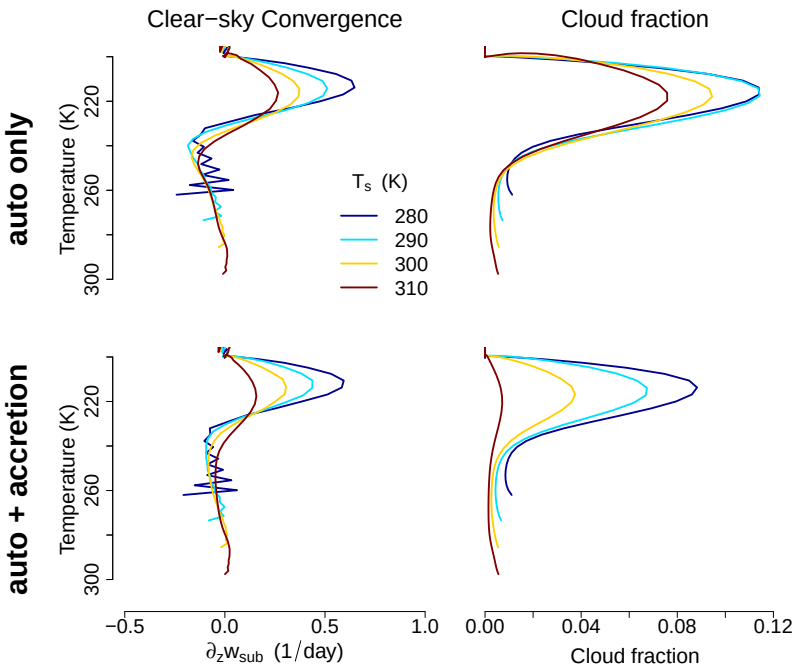

Figure 2. *Similar CSC peaks do not necessarily imply similar anvil cloud fractions.* The top row reproduces the CSC and cloud profiles from Fig. 1, whereas the bottom row shows analogous results from simulations run with warm-rain accretion on. Profiles are again cut off at cloud base for clarity.

portionality. Indeed, a more complex relationship was recently derived by Beydoun et al. (2021), who showed that to first order, the mean anvil cloud fraction $\mathcal{C}$ can be related to CSC as

$$\mathcal{C} \;=\; \mathrm{CSC} \cdot \Delta_h l \cdot \tau \tag{3}$$

where $\Delta_h l$ is a horizontal finite-difference in log cloud condensate across the anvils, and τ is an inverted sum of microphysical and vertical advection time tendencies for log cloud condensate. This relationship shows that cloud fraction is determined not only by CSC, which must obey Eq. (2), but also by microphysical degrees of freedom which are largely unconstrained. Indeed, these extra degrees of freedom explain how CSC can change sign, yet still be tied via Eq. (3) to positive-definite cloud fraction; all that is needed is an accompanying sign change in τ. Such a sign change might even be anticipated, as microphysical processes transition from being a source of cloud condensate in the lower troposphere (via condensation) to a sink in the upper troposphere (via sedimentation).

To emphasize that the microphysical degrees of freedom in Eq. (3) prevent a 1-1 relationship between cloud fraction and CSC, we re-run our simulations with not only warm-rain autconversion (the default setting) but also an additional, widely-used accretion process which converts cloud condensate to rain (Y.-L. Lin et al., 1983, Eq. 51). Profiles of CSC and cloud fraction from these simulations are shown in Fig. 2. These profiles demonstrate explicitly that similar CSC profiles do not imply similar cloud fraction profiles.

These results suggest that even if CSC is a leading-order control on cloud fraction, the presence of largely unconstrained microphysical degrees of freedom limits the predictive power of Eq. (3). In particular, CSC decreases with warming might *typically* lead

to anvil area decreases with warming, but this is not guaranteed to be the case. This is consistent with the aforementioned RCEMIP result that roughly 2/3 of models exhibit a stability iris-effect, but 1/3 do not. Similarly, Beydoun et al. (2021) found an overall stability-iris effect in analyzing RCE simulations over a large SST range, but found the connection between CSC and anvil area to be non-monotonic within their SST range. These results from the literature, along with the results shown here, suggest that Rule 1 is a general tendency of models, but is not entirely robust.

Another formalism for cloud fraction was introduced by Seeley et al. (2019, hereafter S19), who expressed cloud fraction as a product of *gross* detrainment and a positive-definite cloud lifetime. Gross detrainment is not as easily constrained as net detrainment/CSC, but S19's cloud lifetime can be more simply interpreted as a positive-definite lifetime of detrained cloud condensate. Regardless of these differences, however, the implication of the S19 formalism is similar: microphysical timescales play a leading-order role along with detrainment, so changes in detrainment alone may be insufficient to predict changes in anvil area.

3 Mass flux profiles

Another view of decreasing convection with warming focuses on profiles of convective mass flux M. We again begin with the subsidence vertical velocity $w_{\rm sub}$ from Eq. (1), and note that the convective mass flux M must be equal and opposite to the subsidence mass flux $\rho w_{\rm sub}$. Next, we would like to rewrite $w_{\rm sub}$ in a more convenient form. Noting that $\mathcal{H}_{\rm rad} = \frac{g}{C_p}\partial_p F$ (where F is the net upward radiative flux), and then multiplying the numerator and denominator in Eq. (1) by $\rho C_p/\Gamma$, yields after some manipulation

$$M \;=\; -\rho w_{\rm sub} \;=\; \frac{-\partial_T F + \frac{Le}{\Gamma}}{g\left(\frac{1}{\Gamma} - \frac{1}{\Gamma_d}\right)} \tag{4}$$

where e (and later c) is the domain-mean evaporation (condensation) in kg/m^3/s. Next we note that by local energy balance we have $L(c-e) = \partial_z F$ [see also Eq. (10) below], and we also define a local 'conversion efficiency' $\alpha \equiv (c-e)/c$. Combining these relations, one can rewrite Eq. (4) as

$$M \;=\; \frac{1}{\alpha}\frac{-\partial_T F}{g\left(\frac{1}{\Gamma} - \frac{1}{\Gamma_d}\right)} \;. \tag{5}$$

The advantage of this form is that if we use temperature as a vertical coordinate, the numerator becomes tightly constrained: Jeevanjee and Romps (2018) showed, on both theoretical grounds and with cloud-resolving RCE simulations, that the profile $(-\partial_T F)(T)$ is '$T_{\rm s}$-invariant', i.e. the profile does not depend on $T_{\rm s}$. In contrast, the factor of $(1/\Gamma - 1/\Gamma_d)^{-1}$ is quite sensitive to $T_{\rm s}$; indeed its upper-tropospheric peak near $T = 220$ K increases at almost a doubling for every 10 K of surface warming, approximately equal to Clausius-Clapeyron scaling (Fig. A1b). Thus, barring significant changes in the conversion efficiency α (which we do not find, Fig. A1c), we expect the stability-related increases in $(1/\Gamma - 1/\Gamma_d)^{-1}$ with warming to dominate changes at a given isotherm, hence

> **Rule 2**: *Convective mass flux profiles $M(T)$ should decrease at all isotherms with surface warming.*

This prediction of Eq. (5) is confirmed for our simulations in Figure 3a, for both the subsidence mass flux $-\rho w_{\rm sub}$ diagnosed via Eq. (1) as well as the conditionally sampled convective mass flux M (these independently diagnosed profiles are fairly similar, again as required by mass continuity). As per Rule 2, the profiles in Fig. 3a are plotted in temperature coordinates, in which they exhibit a clean decrease with warming at

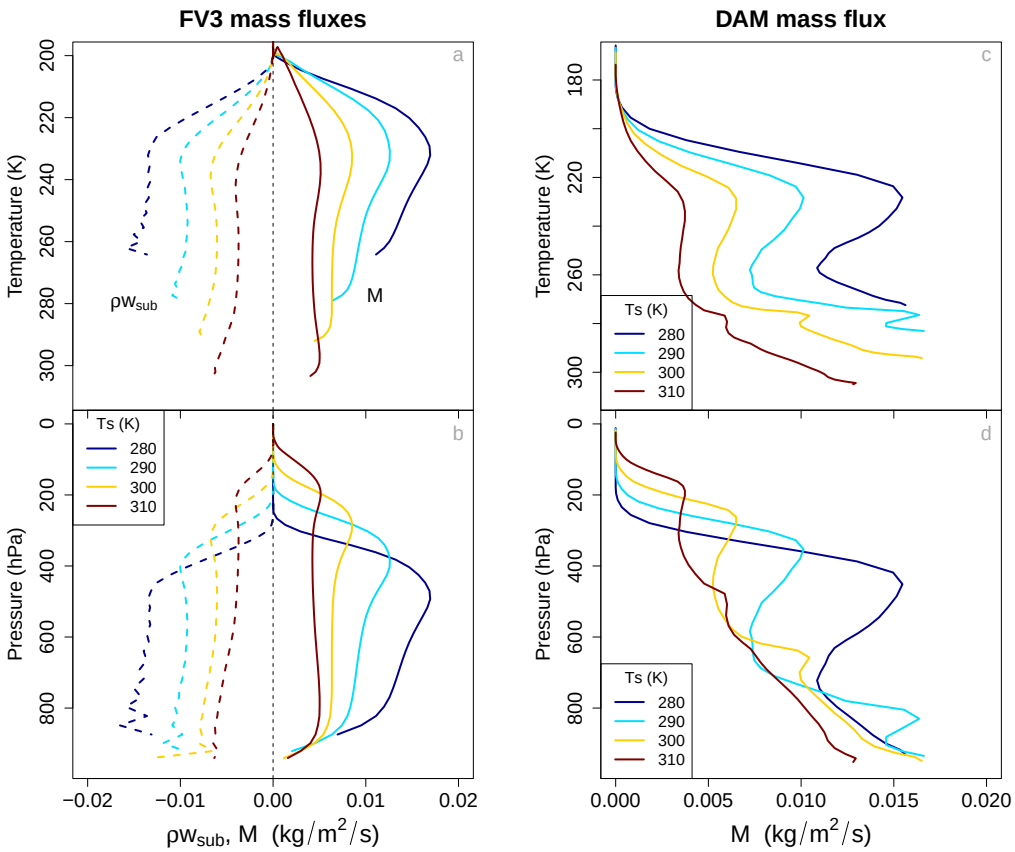

Figure 3. *Mass fluxes decrease with warming throughout the free troposphere, most robustly when plotted in temperature coordinates.* Panel a shows that both (minus) the subsidence mass flux $-\rho w_{\text{sub}}$ and the convective mass flux M, which are independently diagnosed, decrease at essentially all isotherms due to surface warming. This decrease is not evident in the upper troposphere when pressure coordinates are used (panel b). Panels c,d show analogous results, but from higher complexity DAM simulations.

essentially all levels (profiles are, however, cut-off near cloud base for clarity; the behavior of cloud-base M is discussed in the next section). Fig. 3b, on the other hand, shows these profiles in the usual pressure coordinates; in this case, the decrease of M and ρw_{sub} with warming fails in the upper troposphere. Thus, the decrease of upper-tropospheric M with warming depends on the choice of vertical coordinate.

The strong theoretical foundation and encouraging validation of Rule 2 make it a candidate for a robust response of tropical convection to global warming. But, this validation has so far only taken place in the context of an idealized, limited-area cloud-resolving model, so further validation across the model hierarchy is required (Jeevanjee et al., 2017). To this end, we first reproduce Fig. 3a,b but using DAM simulations; the results are shown in Fig. 3c,d. These simulations feature interactive radiation and comprehensive microphysics, yet still show a clean decrease of M at virtually all isotherms (Fig. 3c), again in contrast to the picture in pressure coordinates (Fig. 3d).

Next, we validate Rule 2 in a GCM. We use a 1%CO_2 run of GFDL's CMIP6-generation coupled model CM4, from which monthly mean parameterized convective mass flux profiles M_c were saved (see M. Zhao et al., 2018, for details of CM4's 'double-plume' con-

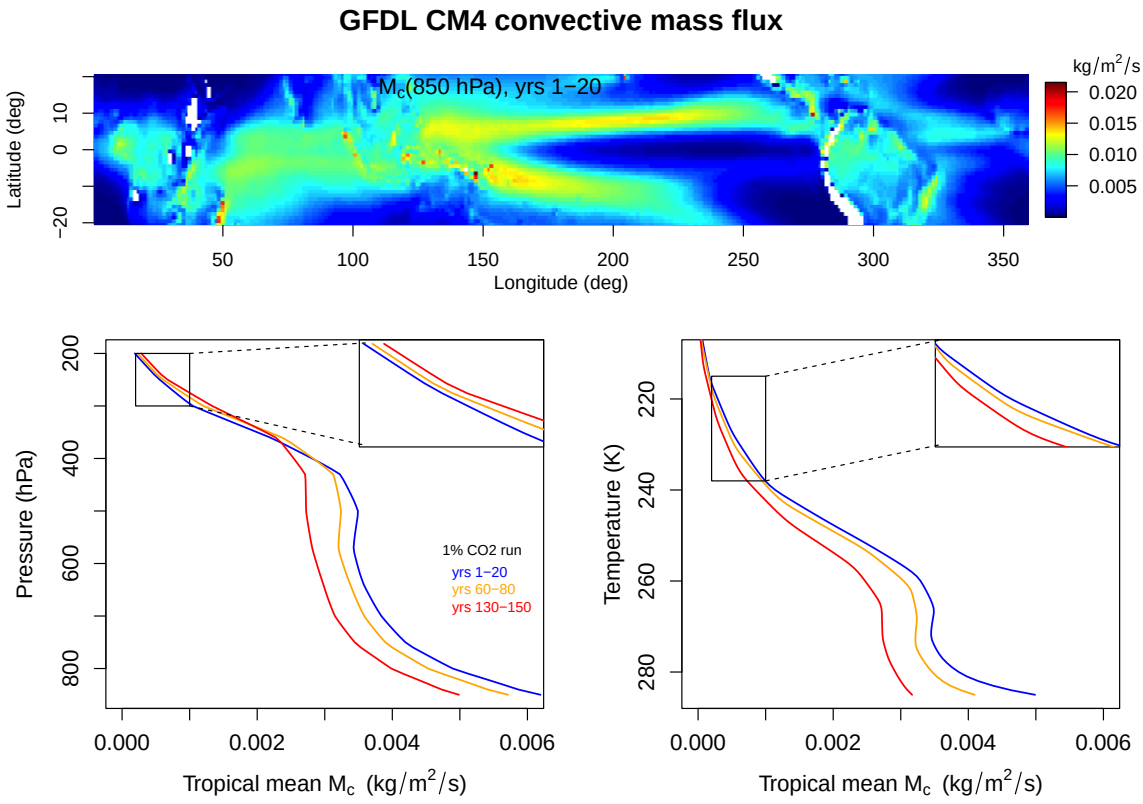

Figure 4. *Tropical-mean mass fluxes from a GCM behave similarly to the RCE results.* This figure shows the parameterized convective mass flux M_c from a 1%CO_2 run of GFDL's CM4 coupled model. The top panel shows a map of M_c(850 hPa) averaged over years 1-20 of the simulation, while the bottom panels show tropical mean (20°S - 20°N) profiles averaged in both pressure and temperature coordinates over years 1-20, 60-80, and 130-150. Despite the complexity evident in the top panel, the tropical mean M_c profiles also decrease robustly throughout the free troposphere, particularly when plotted in temperature coordinates. The insets in the bottom panels show that the *sign* of the mass flux change depends on the choice of vertical coordinate.

vective parameterization). Figure 4 shows a map of time-averaged M_c evaluated at 850 hPa, as well as tropical mean (20°S - 20°N) profiles averaged in both pressure and temperature coordinates over years 1-20, 60-80, and 130-150. The map shows the marked spatial heterogeneity of M_c, similar to the pattern of tropical rainfall. Despite this complexity, however, the tropical mean profiles behave similarly to those from our RCE simulations: M_c decreases with warming throughout the troposphere, and this decrease occurs at all levels in temperature coordinates but not in pressure coordinates. In fact, the insets show that in the upper troposphere, the use of pressure coordinates actually *changes the sign* of the M_c response to warming, further underscoring the importance of the choice of vertical coordinate.

The fact that upper tropospheric M (on fixed isotherms) decreases robustly with warming can actually be seen as the basis for Rule 1: if we know that upper-tropospheric mass fluxes decrease, then it follows fairly naturally that their detrainment should also decrease. Indeed, the changes in stability which drive the decrease in M [cf. Eq. (5)] are the same changes which are thought to drive the changes in the CSC peak under the stability-iris hypothesis (Section 2).

4 Cloud-base mass flux

A third perspective on decreasing convection with warming, first formulated by A. Betts (1998) and later reiterated in a slightly different form by Held and Soden (2006), begins by noting that the cloud-base (or lifting condensation level) convective latent heat flux should equal the mean precipitation, or equivalently the column-integrated free tropospheric radiative cooling $Q_{\rm ft}$ (W/m^2). Mathematically, this is expressed as

$$(Lq_{\rm v}^* M)|_{\rm LCL} \;=\; Q_{\rm ft}. \tag{6}$$

From this it follows that the cloud-base mass flux $M|_{\rm LCL}$ should decrease with warming, because $Q_{\rm ft}$ increases by 1-3%/K (e.g. Jeevanjee & Romps, 2018) whereas $q_{\rm v}^*|_{\rm LCL}$ increases by 7%/K. We thus obtain a third rule, which we refer to as 'Betts's rule':

> **Rule 3 (Betts's rule)**: *Cloud-base convective mass fluxes $M|_{\rm LCL}$ should decrease with surface warming.*

This rule was confirmed in a particular GCM by Held and Soden (2006) (although they used mass fluxes evaluated at 500 hPa rather than cloud-base). On the other hand, Schneider et al. (2010) evaluated the constraint Eq. (6) (their Eq. 8b), and found only middling agreement with their GCM simulations. Here, we can make a qualitative, eyeball evaluation using the mass flux profiles we have already seen: the FV^3 profiles in Fig. 3b seem consistent with Betts's rule, but the DAM profiles in Fig. 3d do not, instead exhibiting non-monotonic changes in M with warming below 800 hPa or so.

These mixed results suggest that Betts's rule is not robust. But, how can the simple argument leading to Eq. (6) fail? And how does Betts's rule connect to our previous rules? We argue here that Betts's rule may not be robust because it assumes that all water vapor lofted above cloud-base both condenses and precipitates to the surface. In other words, Eq. (6) ignores detrainment of water vapor, and also assumes unit precipitation efficiency. We will analytically derive a generalization of Betts's rule from our fundamental equation (1) which accounts for these effects, and show that the associated terms are poorly constrained and plausibly lead to the behavior seen in Fig. 3.

We begin by rewriting Eq. (1) in terms of a flux divergence in z coordinates:

$$M \;=\; \frac{\partial_z F + Le}{C_p(\Gamma_d - \Gamma)}\ . \tag{7}$$

Next, we note that for a saturated, convecting parcel experiencing fractional entrainment per unit distance ϵ (m^{-1}), its saturated moist static energy (MSE) h^* evolves as (Singh & O'Gorman, 2013)

$$\partial_z h^* \;=\; -\epsilon(1-{\rm RH})Lq_{\rm v}^*\ . \tag{8}$$

This expression captures the effect of MSE dilution by mixing with subsaturated environmental air. Using the definition $h^* = C_pT + gz + Lq_{\rm v}^*$, and with some manipulation, this can be re-written as

$$C_p(\Gamma_d - \Gamma) \;=\; -L\underbrace{\left[\frac{dq_{\rm v}^*}{dz} - \epsilon(1-{\rm RH})q_{\rm v}^*\right]}_{c/M}\ . \tag{9}$$

This equation has lapse rates on one side and terms involving $q_{\rm v}^*$ on the other, thus yielding the promised connection between moisture and stability. Furthermore, bulk-plume models of the atmosphere show that the domain-mean condensation rate $c = M[-\partial_z q_{\rm v}^* - \epsilon(1-{\rm RH})q_{\rm v}^*]$ [e.g. Eq. 13 of Romps (2014)], and thus the right-hand side of Eq. (9) is

simply $-Lc/M$. Since the difference $\Gamma_d - \Gamma$ from the left-hand side of Eq. (9) also appears in Eq. (7), we may substituting and rearrange, recovering our statement of local energy balance

$$\partial_z F \;=\; L(c-e)\;. \tag{10}$$

If we now define the precipitation efficiency PE as the ratio of vertically-integrated net condensation to gross condensation, then c and e are related to the precipitation efficiency as

$$PE \;=\; \frac{\int (c-e)dz}{\int c\,dz}\;. \tag{11}$$

Thus, integrating Eq. (10) over the free troposphere, i.e. from the lifting condensation level $z_{\rm LCL}$ to the tropopause height $z_{\rm tp}$, and noting that $\int_{z_{\rm LCL}}^{z_{\rm tp}} \partial_z F\, dz = Q_{\rm ft}$, we obtain

$$Q_{\rm ft} = \; L\int_{z_{\rm LCL}}^{z_{\rm tp}} (c-e)\,dz = \; L\,{\rm PE}\int_{z_{\rm LCL}}^{z_{\rm tp}} c\,dz = \; L\,{\rm PE}\int_{z_{\rm LCL}}^{z_{\rm tp}} \left(-M\frac{dq_{\rm v}^*}{dz} - \epsilon M(1-{\rm RH})q_{\rm v}^*\right) dz\;.$$

The key step is to now integrate by parts on the right-hand side of this equation. Neglecting $q_{\rm v}^*(z_{\rm tp})$ eliminates one of the boundary terms, and invoking $\partial_z M = \epsilon M - \delta M$ where δ is gross fractional detrainment then yields finally

$$(Lq_{\rm v}^*\,{\rm PE}\,M)|_{\rm LCL} \;+\; \underbrace{L\,{\rm PE}\int_{z_{\rm LCL}}^{z_{\rm tp}} [-\delta M + \epsilon M {\rm RH}]q_{\rm v}^*\,dz}_{\text{entrainment/detrainment term}} \;=\; Q_{\rm ft}\;. \tag{12}$$

This equation is the generalization of Eq. (6) we seek: it accounts for non-unit precipitation efficiency, and through the 'entrainment/detrainment' term accounts for possible changes in the moisture flux due to entrainment/detrainment of water vapor in the free troposphere. Equation (12) is thus more complete than Eq. (6), but also potentially much less robust, particularly due to the entrainment/detrainment term which seems difficult to constrain theoretically. Indeed comparison of the FV^3 mass-flux profiles in Fig. 3a,b , which tend to increase somewhat with height through the lower-mid troposphere, to the DAM mass-flux profiles in Fig. 3c,d, which tend to decrease with height rather markedly below the freezing point, suggests that entrainment and detrainment even in RCE are not easily constrained.

One might hold out hope, however, that the entrainment/detrainment term might be negligible compared to the cloud-base term; if true, this would yield a more viable constraint of

$$(Lq_{\rm v}^*\,{\rm PE}\,M)|_{\rm LCL} \;\approx\; Q_{\rm ft}\;. \tag{13}$$

We wish to test how well this version of Eq. (6), which differs only by accounting for $PE \neq 1$, can predict changes in $M|_{\rm LCL}$ with warming. This will require diagnosis of all factors in Eq. (13) besides $M|_{\rm LCL}$, from both our FV^3 and DAM simulations. We diagnose $M|_{\rm LCL}$ as an average of M between 800 and 850 hPa, diagnose $q_{\rm v}^*|_{\rm LCL}$ as $q_{\rm v}$ at the 2nd lowest model level (this is characteristic of the boundary-layer values and thus of saturated parcels at cloud-base), diagnose $Q_{\rm ft}$ as the radiative cooling integrated from cloud-base to the tropopause, and diagnose precipitation efficiency according to Eq. (11).

With these diagnostics in hand, Figure 5 compares the directly diagnosed $M|_{\rm LCL}$ to $M|_{\rm LCL}$ as estimated from both Eq. (13) and Eq. (6) by solving for $M|_{\rm LCL}$. Consistent with the results of Schneider et al. (2010), this figure shows that while the theoretical estimates gives reasonable ballpark values for $M|_{\rm LCL}$, especially when non-unit PE is accounted for, they predict a decreasing trend which is only very roughly obeyed by the models. FV^3 does shows a decreasing trend, but its slope is less than half of that estimated from Eq. (13). Meanwhile DAM shows a non-monotonic change of $M|_{\rm LCL}$ with $T_{\rm s}$, as indicated earlier. Thus, the entrainment/detrainment terms in Eq. (12) seem to play a non-negligible role in the change of $M|_{\rm LCL}$ with warming, inhibiting the robustness of Betts's rule. Inclusion of PE helps obtain more accurate values overall, but *changes*

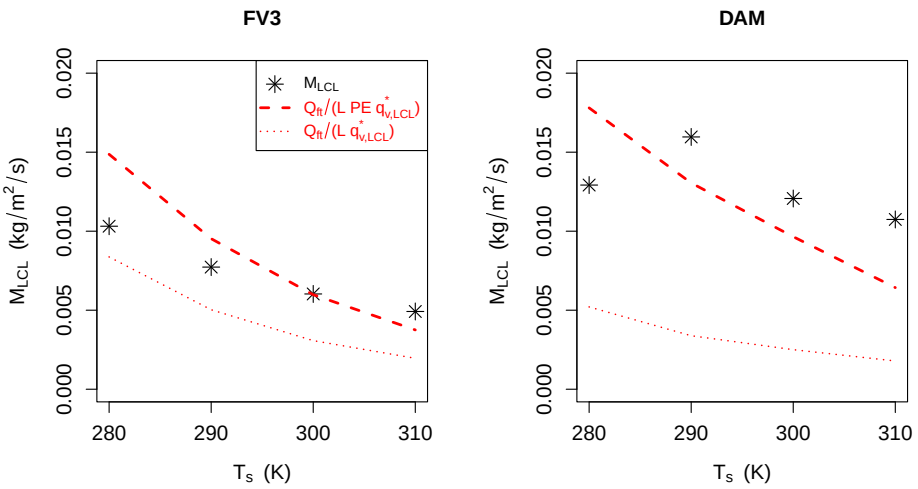

Figure 5. *Cloud-base mass fluxes do not closely follow the constraint Eq. (13).* These panels show cloud-bass mass fluxes $M|_{\mathrm{LCL}}$ plotted against surface temperature T_{s}, for both our FV^3 and DAM simulations. Markers denote $M|_{\mathrm{LCL}}$ diagnosed directly from simulations, whereas red dashed and dotted lines denote estimates obtained from Eq. (13) and Eq. (6), respectively. The non-unit PE in Eq. (13) yields more accurate estimates overall, but the predicted slope is too steep in FV^3 and does not capture the non-monotonicity of $M|_{\mathrm{LCL}}$ in DAM.

in PE with warming are small (varying between 0.56-0.51 in FV^3, and 0.26-0.3 in DAM) and thus do not impact the response of $M|_{\mathrm{LCL}}$.

It is worth noting that in the original formulation of A. Betts (1998), the constraint on $M|_{\mathrm{LCL}}$ is formulated with an additional RH-dependent term. This formulation is derived and discussed in Appendix C.

5 Implications (or not) for large-scale circulations

A topic left unaddressed so far are the implications of these rules for changes in the tropical large-scale circulation, especially the Hadley and Walker circulations. These implications are not straightforward, for a number of reasons.

Firstly, for a large-scale vertical velocity field w discretized over a $O(100$ km) horizontal grid spacing typical of GCMs or reanalyses, the analog of the convective mass flux M considered here would be the tropical-average gross upward mass flux $\overline{M}_{\mathrm{up}} \equiv \rho \overline{w}_{\mathrm{up}} \sigma_{\mathrm{up}}$, where σ_{up} is the average fraction of tropical grid cells with $w > 0$ and $\overline{w}_{\mathrm{up}}$ is the conditional average of w over those grid cells. For this quantity to be analogous to M, and to obey the constraint (5), it is necessary that the conditional sampling be performed column-wise and over short enough time scales that w does not change sign in a given column. If either of these conditions are relaxed, upward and downward motions can compensate to yield an underestimate.

Even if $\overline{M}_{\mathrm{up}}$ profiles are properly calculated and seen to decrease with warming, similarly to M (e.g. Fig 2e of Jenney et al., 2020), it can be difficult to then draw conclusions about $\overline{w}_{\mathrm{up}}$ and σ_{up} since these can vary independently. For instance, Vecchi and Soden (2007) (using monthly-mean w) found a robust and significant decrease in 500 hPa $\overline{w}_{\mathrm{up}}$ across CMIP3 GCMs, whereas Jenney et al. (2020) found only weak reductions in

$\overline{w}_{\rm up}$, but strong reductions in $\sigma_{\rm up}$, using a super-parameterized GCM run in a global RCE configuration.

Furthermore, for large-scale tropical circulations such as the Hadley and Walker circulation, circulation strength is typically measured by a streamfunction which requires temporal and spatial averaging over columns which, even in an ascending branch, can exhibit both positive and negative values of w. This averaging and ensuing compensation yields a *net* upward mass flux which can be several-fold smaller than the gross upward mass flux $\overline{M}_{\rm up}$ (Schneider et al., 2010). Thus, the constraint (5) is not directly applicable to streamfunction-estimated mass fluxes.

Another consequence of this averaging is that even if $\overline{M}_{\rm up}$, $\overline{w}_{\rm up}$, and $\sigma_{\rm up}$ were fixed with warming, spatial *redistributions* of the w field can yield large changes in the streamfunction, by simply changing how positive and negative values of w compensate under time averaging. An extreme example of this would be to completely randomize the location of convection, as in the unorganized RCE simulations considered here, in which case the time-averaged large-scale circulation disappears entirely, despite the presence of nonzero M (Held & Soden, 2006). Another example of this are ENSO oscillations, which yield changes in the Walker circulation driven almost entirely by redistribution of convection rather than changes in $\overline{M}_{\rm up}$ or $\overline{w}_{\rm up}$. A final example is the observed *strengthening* of the Walker circulation over the last few decades, which cannot be due to the small expected decrease in $\overline{M}_{\rm up}$ over that period and instead must arise from a redistribution of convection, likely linked to the pattern of SST warming over that period (e.g. Ma & Zhou, 2016; X. Zhao & Allen, 2019).

6 Summary and Discussion

This paper has shown that

- Three rules for the decrease of convection with warming can be formulated, each of which spring from Eq. (1) and thus embody the same physics
- The stability-iris effect (Rule 1) is not entirely robust because clear-sky convergence and cloud fraction are not directly proportional, but rather are connected by loosely constrained microphysical process [Eq. (3) and Figs. 1 and 2]
- The decrease in tropospheric mass flux on isotherms (Rule 2) does seem to be potentially robust, based on its theoretical foundation [Eq. (5)] as well as validation across a hierarchy of models (Figs. 3 and 4)
- The decrease in cloud-base mass fluxes (Rule 3) is not entirely robust, due to the loosely constrained effects of entrainment and detrainment [Eq. (12) and Fig. 5].

Our three rules, along with the analytical constraints from which they are deduced, are summarized in Table 1. It is worth noting that these constraints are all related by integration/differentiation: indeed, the constraint (2) is obtained by differentation of Eq. (1), the constraint (5) is simply a re-arrangement of Eq. (1), and the constraint (13) is obtained from Eq. (1) via integration by parts.

What are the broader implications of these findings? The lack of robustness of the stability-iris hypothesis as a potential mechanism for the tropical anvil cloud area feedback has been noted before (Sherwood et al., 2020). But, our emphasis on the microphysical degrees of freedom suggests that uncertainties in this feedback may not be easily remedied, as microphysical complexity is daunting (e.g. Fig. 1 of Morrison et al., 2020) and high clouds appear to be sensitive to many aspects of this complexity (e.g. evolution of various ice species, sedimentation, sub-grid scale saturation adjustment, Ohno & Satoh, 2018; Ohno et al., 2020, 2021).

Table 1. Summary of the three rules and their corresponding constraints.

Rule	**Constraint**
(Stability-iris) Clear-sky convergence, convective detrainment, and anvil cloud fraction decrease together with warming	$\mathrm{CSC} \;=\; \partial_z \left(\dfrac{\mathcal{H}_{\mathrm{rad}} + \mathcal{H}_{\mathrm{e}}}{\Gamma_d - \Gamma} \right)$
Convective mass fluxes decrease at all isotherms with surface warming	$M \;=\; \dfrac{1}{\alpha} \dfrac{-\partial_T F}{g \left(\frac{1}{\bar{\Gamma}} - \frac{1}{\Gamma_d} \right)}$
(Betts's rule) Cloud-base convective mass fluxes decrease with surface warming	$(L q_{\mathrm{v}}^* \,\mathrm{PE}\, M)\vert_{\mathrm{LCL}} \;\approx\; Q_{\mathrm{ft}}$

As for the decrease of mass flux profiles with warming: this is a straightforward consequence of decreasing w_{sub} with warming, which is well-known, but an explicit confirmation of this for *profiles* of M, rather than just mid-tropospheric M, was to our knowledge first provided only recently by Jenney et al. (2020). Here, we have also emphasized the importance of temperature coordinates, and leveraged the T_{s}-invariance of $\partial_T F$ to put the decrease of M on a stronger theoretical footing [Eq. (5)].

As for Betts's rule (Rule 3), this has long been invoked as a mechanism behind the weakening of tropical circulations, particularly the Walker circulation (e.g. Vecchi & Soden, 2007). However, as discussed in Section 5, even if one were to invoke the better justified Rule 2 as a mechanism, there are many issues complicating the connection to large-scale circulations. Future work could untangle these issues and examine the degree to which Rule 2 truly implies a tendency of large-scale circulations to weaken.

Finally, it is worth reflecting on the essential physics behind our rules. The physics behind Betts's Rule is straightforward enough: cloud-base moisture increases faster than column-integrated radiative cooling, so less mass flux is required. But are there analogous statements for Rules 1 and 2? The driving force there seems to be the increasing difference between $\Gamma(T)$ and Γ_d, particularly in the upper troposphere, as T_{s} increases (Fig. A1a,b). What causes this? Even at a fixed upper-tropospheric isotherm T, $q_{\mathrm{v}}^*(T)$ will still increase with T_{s} because the *pressure* and hence ambient air density are going down, even if the vapor pressure is not changing. This actually causes a quasi-exponential increase of $q_{\mathrm{v}}^*(T)$ with T_{s}, even though the isotherm T is fixed (see detailed discussion in Romps, 2016). This increase of $q_{\mathrm{v}}^*(T)$ then increases the latent heating of ascending parcels, leading to an increase in stability measures such as $1/\Gamma - 1/\Gamma_d$. Meanwhile, the $-\partial_T F$ factor in Eq. (5) is T_{s}-invariant. Thus, Rule 2 (and also Rule 1, as a derivative of Rule 2) is again driven by a mismatch between the scalings of radiative cooling and moisture with T_{s}. This is reminiscent of Mapes's 'two scale-heights' argument (Mapes, 2001), but applied to global warming rather than our base climate.

Appendix A FV^3 Simulations

The atmospheric model used here is the non-hydrostatic version of GFDL's FV^3 (Finite-Volume Cubed-Sphere Dynamical Core, Harris & Lin, 2013; S.-J. Lin, 2004). The simulations analyzed here are very similar to those of Jeevanjee and Zhou (2022), so we describe some salient aspects of the simulation below, and refer the reader to Jeevanjee and Zhou (2022) for complete details.

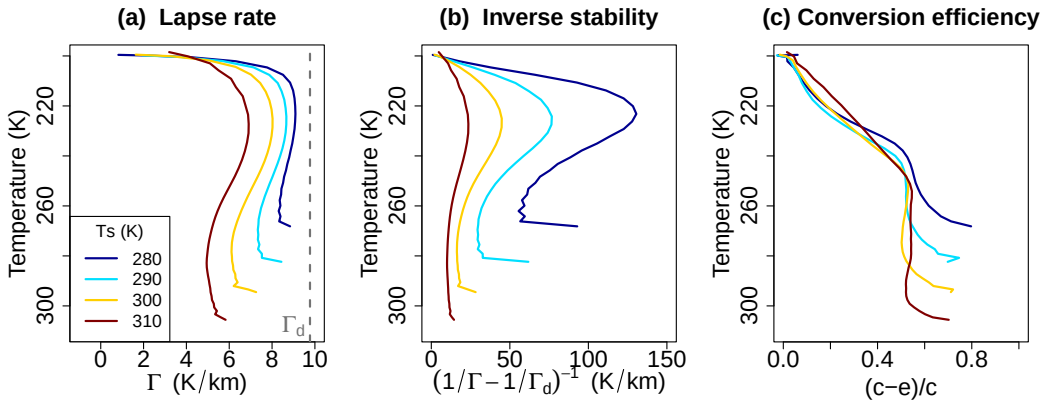

Figure A1. The lapse rate profiles $\Gamma(T)$ decrease with T_s and become more distant from the dry value (panel a), causing a marked increase in the inverse stability parameter $(1/\Gamma - 1/\Gamma_d)^{-1}$ (panel b). Meanwhile, profiles of conversion efficiency are roughly T_s-invariant (panel c).

We simulate doubly-periodic radiative-convective equilibrium (RCE) over fixed sea surface temperatures of T_s=280, 290, 300 and 310 K. Our particular FV^3 codebase is not equipped with interactive radiation, so radiative cooling must be otherwise parameterized. To emulate the T_s-dependence of interactive radiation, we parameterized it as a fit to the invariant divergence of radiative flux F found by Jeevanjee and Romps (2018):

$$-\partial_T F = (0.025 \text{ W/m}^2/\text{K}^2) \cdot (T - T_{tp}) \ . \tag{A1}$$

Here the temperature derivative is a vertical derivative and $T_{tp} = 200$ K is the tropopause temperature. Above the tropopause temperatures are relaxed to T_{tp}, so the stratosphere is roughly isothermal. The invariance of $(-\partial_T F)(T)$ profiles with respect to T_s was shown on both theoretical grounds and with cloud-resolving simulations in Jeevanjee and Romps (2018), and also confirmed across cloud-resolving models in Stauffer and Wing (2022).

No boundary layer or sub-grid turbulence schemes are used. Microphysical transformations are performed with a warm-rain version of the GFDL microphysics scheme (Zhou et al., 2019; Chen & Lin, 2013), which in its default configuration models only water vapor q_v (kg/kg), cloud condensate, and rain, with the only transformations being condensation/evaporation of condensate and autoconversion of cloud condensate to rain (rain evaporation is disabled). The horizontal grid has 96 points in both x and y with a resolution of 1 km, and the 90-level vertical grid has a stretched grid spacing of 50 m near the surface up to 5000 m near model top at 68 km. Each simulation ran for 120 days, with domain-mean statistics drawn from the last 5 days.

Actively convecting (updraft) grid cells are identified as having cloud condensate mixing ratios greater than 10^{-5} as well as vertical velocities $w > 0.7$ m/s, and convective mass fluxes are then defined at each level as $M \equiv \rho w_{up} \sigma_{up}$ (kg/m^2/s) where w_{up} is w conditionally averaged over updraft grid cells, and σ_{up} is the fractional area occupied by updraft grid cells. Cloud-base is defined as the lower-level maximum in cloud fraction, and the tropopause is defined as the lowest model within 0.5 K of $T_{tp} = 200$ K. Figure A1 shows three key diagnostics for the arguments presented in this paper: the lapse rate Γ, inverse stability parameter $(1/\Gamma - 1/\Gamma_d)^{-1}$, and conversion efficiency $\alpha = (c - e)/c$.

Appendix B DAM Simulations

Our second set of cloud-resolving RCE simulations use Das Atmosphärische Modell (DAM, Romps, 2008), a fully-compressible, non-hydrostatic cloud-resolving model, coupled to radiation via the comprehensive Rapid Radiative Transfer Model (RRTM, Mlawer et al., 1997). DAM employs the six-class Lin-Lord-Krueger microphysics scheme (Y.-L. Lin et al., 1983; Lord et al., 1984; Krueger et al., 1995), and in contrast to its original formulation in Romps (2008) employs no explicit sub-grid scale turbulence scheme, relying instead on 'implicit LES' for sub-grid scale transport (Margolin et al., 2006).

These simulations ran on a square doubly-periodic domain of horizontal dimension $L = 72$ km, with a horizontal grid spacing of $dx = 1$ km. The 76 level vertical grid has a spacing which stretches smoothly from 50 m below 1000 m to 250 m between 1000 m and 5000 m, and then to 500 m up to the model top at 30 km. We calculated surface heat and moisture fluxes using simple bulk aerodynamic formulae, and used a pre-industrial CO_2 concentration of 280 ppm with no ozone. Our SSTs are the same as for the FV^3 simulations, and all our DAM runs branched off the equilibrated runs described in Romps (2014) and were run for 60 days to iron out any artifacts from changing the domain and resolution. All vertical profiles are time-mean and domain-mean, averaged over the last 5 days of each run. All diagnostics are constructed identically to their FV^3 counterparts, except the vertical velocity threshold for conditional sampling of convective mass flux is taken to be 1 m/s.

Appendix C Betts's Original Rule

The original formulation of Betts's rule (A. Betts, 1998) reads (assuming precipitation equals $Q_{\rm ft}$)

$$Q_{\rm ft} \;=\; L[M(1-{\rm RH})q_{\rm v}^*]|_{\rm LCL}\;. \tag{C1}$$

Unlike the version (6) appearing in Held and Soden (2006), this constraint can be derived without neglect of entrainment or non-unit PE, as follows. We again turn to the bulk-plume equations, for both in-plume and environmental moisture (e.g. Eqns 8 and 9 of Romps, 2016):

$$\begin{aligned}\partial_z q_{\rm v}^* &= -\epsilon(1-{\rm RH})q_{\rm v}^* - c/M\\ -\partial_z({\rm RH}q_{\rm v}^*) &= \delta(1-{\rm RH}) + (1-\alpha)c/M\end{aligned}$$

(note that our α equals $1-\alpha$ in Romps (2016)). Adding these equations and noting that $\partial_z M = M(\epsilon-\delta)$, one can rewrite the result as

$$\alpha c = -\partial_z[(1-{\rm RH})Mq_{\rm v}^*]\;. \tag{C2}$$

Integrating Eq. (10) and invoking Eq. (C2) as well as the definition of vertically-resolved $\alpha = (c-e)/c$ rather than PE yields

$$Q_{\rm ft} \;=\; L\int_{z_{\rm LCL}}^{z_{\rm tp}} \alpha c\,dz \;=\; -L\int_{z_{\rm LCL}}^{z_{\rm tp}} \partial_z[(1-{\rm RH})Mq_{\rm v}^*] \;=\; L[(1-{\rm RH})Mq_{\rm v}^*]|_{\rm LCL}\;, \tag{C3}$$

which is Eq. (C1).

Given that this version of Betts's rule does not neglect entrainment/detrainment or evaporation of condensate, one might hope that it might provide a more robust constraint on $M|_{\rm LCL}$ than Eq. (6). But, we have already seen that $M|_{\rm LCL}$ does not always decrease with warming (Fig. 3c). Thus, there must be an unconstrained parameter in Eq. (C1), which can only be ${\rm RH}|_{\rm LCL}$. Indeed, both our FV^3 and DAM simulations show RH increases of 0.2 over our SST range, yielding significant decreases in $(1-{\rm RH})$. Future work could ask if these changes are predictable, perhaps on the basis of the RH theory of Romps (2014).

Open Research

Data and scripts used in generation of the figures in this paper will be available upon publication with doi 10.5281/zenodo.6792098. Data are available for reviewer use at

https://www.dropbox.com/sh/ec5zl3r6scf1b22/AADATrM0gHslrStF_XEj1y2ra?dl=0.

Acknowledgments

The author thanks Linjiong Zhou for help with configuring cloud-resolving simulations with FV^3 and for development of the warm-rain option of the GFDL microphysics package. Jake Seeley, Zhihong Tan, and Linjiong Zhou provided valuable feedback on early drafts of this work. Yi Ming provided encouragement and suggested the use of GFDL CM4 output.

References

Betts, A. (1998). Climate-Convection Feedbacks: Some Further Issues. *Climatic Change*, *39*(1), 35–38.

Betts, A. K., & Ridgway, W. (1989). *Climatic equilibrium of the atmospheric convective boundary layer over a tropical ocean* (Vol. 46) (No. 17).

Beydoun, H., Caldwell, P. M., Hannah, W. M., & Donahue, A. S. (2021). Dissecting Anvil Cloud Response to Sea Surface Warming. *Geophysical Research Letters*, *48*(15), 1–11.

Bony, S., Stevens, B., Coppin, D., Becker, T., Reed, K. A., Voigt, A., & Medeiros, B. (2016). Thermodynamic control of anvil cloud amount. *Proceedings of the National Academy of Sciences of the United States of America*, *113*(32), 8927–8932.

Chen, J. H., & Lin, S. J. (2013). Seasonal predictions of tropical cyclones using a 25-km-resolution general circulation model. *Journal of Climate*, *26*(2), 380–398.

Cronin, T. W., & Wing, A. A. (2017). Clouds, Circulation, and Climate Sensitivity in a Radiative-Convective Equilibrium Channel Model. *Journal of Advances in Modeling Earth Systems*, 2883–2905.

Harris, L. M., & Lin, S.-J. (2013, jan). A Two-Way Nested Global-Regional Dynamical Core on the Cubed-Sphere Grid. *Monthly Weather Review*, *141*(1), 283–306.

Hartmann, D. L., Blossey, P. N., & Dygert, B. D. (2019). Convection and Climate: What Have We Learned from Simple Models and Simplified Settings? *Current Climate Change Reports*, *5*(3), 196–206.

Hartmann, D. L., & Larson, K. (2002). An important constraint on tropical cloud - climate feedback. *Geophysical Research Letters*, *29*(20), 1951.

Held, I. M., Guo, H., Adcroft, A., Dunne, J. P., Horowitz, L. W., Krasting, J., ... Zadeh, N. (2019). Structure and Performance of GFDL's CM4.0 Climate Model. *Journal of Advances in Modeling Earth Systems*, 1–37.

Held, I. M., & Soden, B. J. (2006). Robust responses of the hydrological cycle to global warming. *Journal of Climate*, *19*, 5686–5699.

Jeevanjee, N., Hassanzadeh, P., Hill, S., & Sheshadri, A. (2017, jul). A perspective on climate model hierarchies. *Journal of Advances in Modeling Earth Systems*, *9*(4), 1760–1771.

Jeevanjee, N., & Romps, D. M. (2018). Mean precipitation change from a deepening troposphere. *Proceedings of the National Academy of Sciences*, *115*(45), 11465–11470.

Jeevanjee, N., & Zhou, L. (2022). On the Resolution-Dependence of Anvil Cloud Fraction and Precipitation Efficiency in Radiative-Convective Equilibrium. *Journal of Advances in Modeling Earth Systems*, *14*(3).

Jenney, A. M., Randall, D. A., & Branson, M. D. (2020). Understanding the Re-

sponse of Tropical Ascent to Warming Using an Energy Balance Framework. *Journal of Advances in Modeling Earth Systems*, *12*(6).

Knutson, T. R., & Manabe, S. (1995). Simulation of the Tropical Pacific Climate with a Coupled Ocean-Atmosphere General Circulation Model. Part I: The Seasonal Cycle. *Journal of climate*, *8*(5), 1178–1198.

Krueger, S. K., Fu, Q., Liou, K. N., & Chin, H.-N. S. (1995, mar). Improvements of an Ice-Phase Microphysics Parameterization for Use in Numerical Simulations of Tropical Convection. *Journal of Applied Meteorology*, *34*, 281–287.

Lin, S.-J. (2004, oct). A 'Vertically Lagrangian' Finite-Volume Dynamical Core for Global Models. *Monthly Weather Review*, *132*(10), 2293–2307.

Lin, Y.-L., Farley, R. D., & Orville, H. D. (1983). *Bulk Parameterization of the Snow Field in a Cloud Model* (Vol. 22) (No. 6).

Lord, S. J., Willoughby, H. E., & Piotrowicz, J. M. (1984, oct). Role of a Parameterized Ice-Phase Microphysics in an Axisymmetric, Nonhydrostatic Tropical Cyclone Model. *Journal of the Atmospheric Sciences*, *41*(19), 2836–2848.

Lutsko, N. J., Sherwood, S. C., & Zhao, M. (2022). Precipitation Efficiency and Climate Sensitivity. , 1–18.

Ma, S., & Zhou, T. (2016). Robust Strengthening and westward shift of the tropical Pacific Walker circulation during 1979-2012: A comparison of 7 sets of reanalysis data and 26 CMIP5 models. *Journal of Climate*, *29*(9), 3097–3118.

Mapes, B. E. (2001). Water's Two Scale Heights: The Moist Adiabat and the Radiative Troposphere. *Quarterly Journal of the Royal Meteorological Society*, *127*(January), 2353–2366.

Margolin, L. G., Rider, W. J., & Grinstein, F. F. (2006, jan). Modeling turbulent flow with implicit LES. *Journal of Turbulence*, *7*, N15.

Mlawer, E. J., Taubman, S. J., Brown, P. D., Iacono, M. J., & Clough, S. A. (1997, jul). Radiative transfer for inhomogeneous atmospheres: RRTM, a validated correlated-k model for the longwave. *Journal of Geophysical Research*, *102*(D14), 16663.

Morrison, H., van Lier-Walqui, M., Fridlind, A. M., Grabowski, W. W., Harrington, J. Y., Hoose, C., ... Xue, L. (2020). *Confronting the Challenge of Modeling Cloud and Precipitation Microphysics* (Vol. 12) (No. 8).

Ohno, T., Noda, A. T., & Satoh, M. (2020). Notes and correspondence impacts of sub-grid ice cloud physics in a turbulence scheme on high clouds and their response to global warming. *Journal of the Meteorological Society of Japan*, *98*(5), 1069–1081.

Ohno, T., Noda, A. T., Seiki, T., & Satoh, M. (2021). Importance of Pressure Changes in High Cloud Area Feedback Due to Global Warming. *Geophysical Research Letters*, *48*(18).

Ohno, T., & Satoh, M. (2018). Roles of Cloud Microphysics on Cloud Responses to Sea Surface Temperatures in Radiative-Convective Equilibrium Experiments Using a High-Resolution Global Nonhydrostatic Model. *Journal of Advances in Modeling Earth Systems*, *10*(8), 1970–1989.

Romps, D. M. (2008). The Dry-Entropy Budget of a Moist Atmosphere. *Journal of the Atmospheric Sciences*, *65*(12), 3779–3799.

Romps, D. M. (2014, oct). An Analytical Model for Tropical Relative Humidity. *Journal of Climate*, *27*(19), 7432–7449.

Romps, D. M. (2016). Clausius-Clapeyron Scaling of CAPE from Analytical Solutions to RCE. *Journal of the Atmospheric Sciences*, *73*(9), 3719–3737.

Saint-Lu, M., Bony, S., & Dufresne, J. L. (2020). Observational Evidence for a Stability Iris Effect in the Tropics. *Geophysical Research Letters*, *47*(14).

Schneider, T., O'Gorman, P., & Levine, X. (2010). Water vapor and the dynamics of climate changes. *Reviews of Geophysics*(48), 1–22.

Seeley, J. T., Jeevanjee, N., Langhans, W., & Romps, D. M. (2019). Formation of Tropical Anvil Clouds by Slow Evaporation. *Geophysical Research Letters*,

46(1), 492–501.

Sherwood, S. C., Webb, M. J., Annan, J. D., Armour, K. C., Forster, P. M., Hargreaves, J. C., ... Zelinka, M. D. (2020). An Assessment of Earth's Climate Sensitivity Using Multiple Lines of Evidence. *Reviews of Geophysics*, *58*(4), 1–92.

Singh, M. S., & O'Gorman, P. A. (2013). Influence of entrainment on the thermal stratification in simulations of radiative-convective equilibrium. *Geophysical Research Letters*, *40*(16), 4398–4403.

Singh, M. S., & O'Gorman, P. A. (2015). Increases in moist-convective updraught velocities with warming in radiative-convective equilibrium. *Quarterly Journal of the Royal Meteorological Society*, *141*(692), 2828–2838.

Stauffer, C. L., & Wing, A. A. (2022). Properties, Changes, and Controls of Deep-Convecting Clouds in Radiative-Convective Equilibrium. *Journal of Advances in Modeling Earth Systems*.

Tsushima, Y., Iga, S. I., Tomita, H., Satoh, M., Noda, A. T., & Webb, M. J. (2014). High cloud increase in a perturbed SST experiment with a global nonhydrostatic model including explicit convective processes. *Journal of Advances in Modeling Earth Systems*, *6*(3), 571–585.

Vecchi, G. A., & Soden, B. J. (2007). Global warming and the weakening of the tropical circulation. *Journal of Climate*, *20*(17), 4316–4340.

Wing, A. A., Stauffer, C. L., Becker, T., Reed, K. A., Ahn, M., Arnold, N. P., ... Zhao, M. (2020). Clouds and Convective Self-Aggregation in a Multi-Model Ensemble of Radiative-Convective Equilibrium Simulations. *Journal of Advances in Modeling Earth Systems*, 1–72.

Zhao, M., Golaz, J.-C., Held, I. M., Guo, H., Balaji, V., Benson, R., ... Xiang, B. (2018). The GFDL Global Atmosphere and Land Model AM4.0/LM4.0: 2. Model Description, Sensitivity Studies, and Tuning Strategies. *Journal of Advances in Modeling Earth Systems*, 735–769.

Zhao, X., & Allen, R. J. (2019). Strengthening of the walker circulation in recent decades and the role of natural sea surface temperature variability. *Environmental Research Communications*, *1*(2).

Zhou, L., Lin, S. J., Chen, J. H., Harris, L. M., Chen, X., & Rees, S. L. (2019). Toward convective-scale prediction within the next generation global prediction system. *Bulletin of the American Meteorological Society*, *100*(7), 1225–1243.